Research on flame temperature measurement method based on water vapor emission spectrum

OPEN ACCESS
IOP Publishing
Measurement Science and Technology
Meas. Sci. Technol. **34** (2023) 054001 (10pp)
https://doi.org/10.1088/1361-6501/acb3e9

Research on flame temperature measurement method based on water vapor emission spectrum

Gongxi Zhou[1,2], Fei Li[2,*], Xin Lin[2], Renjie Li[1,2], Dongdong Meng[2] and Xilong Yu[1,2]

[1] State Key Laboratory of High Temperature Gas Dynamics, Institute of Mechanics, CAS, Beijing 100190, People's Republic of China
[2] School of Engineering Science, University of Chinese Academy of Sciences, Beijing 100049, People's Republic of China

E-mail: lifei@imech.ac.cn

Received 24 August 2022, revised 21 November 2022
Accepted for publication 17 January 2023
Published 31 January 2023

Abstract

Internal temperature monitoring of high-speed propulsion systems is highly important for engine performance evaluation and lifetime prediction. As a passive optical measurement method without the need for an external light source and without flow field interference, the emission spectrum measurement technique has good application prospects for harsh measurement environments. As the main combustion product, high-temperature water vapor shows a strong emission intensity that is highly suitable for temperature measurement applications. We propose use of the band integral ratio to remove the high resolution measurement requirements for the spectrum acquisition system. In addition, the temperatures of methane-oxygen flames with different equivalent ratios are measured successfully under the condition that the influence of self-absorption on the measurements is considered.

Keywords: water vapor spectrum, high temperature measurement, self-absorption, intensity ratio

(Some figures may appear in colour only in the online journal)

1. Introduction

Rapid developments in the aerospace industry are leading to higher requirements for high-temperature gas measurements. Generally, measurement methods for high-temperature gases can be divided into two types: intrusive and non-intrusive. The intrusive measurement method represented by use of a thermocouple can easily induce changes in the flow field, and the upper temperature measurement limit is low, which means that it is unsuitable for use in complex measurement environments.

The non-intrusive optical measurement methods used in the combustion field can be divided into active and passive measurements, depending on whether or not external signals are applied to the combustion. Active measurement methods are represented by absorption spectroscopy, laser-induced fluorescence, and laser scattering techniques [1, 2]. Tunable diode laser absorption spectroscopy (TDLAS) can scan the gas characteristic absorption line pattern accurately by controlling the laser to obtain the relevant flow field parameters. The contribution of Hanson and colleagues to this technology is quite outstanding. They proposed a $2f/1f$ calibration-free method based on residual amplitude modulation that improved the applicability of TDLAS technology greatly [3, 4]. However, because of the complexity of the experimental environment, it is difficult to obtain effective experimental data from engines using TDLAS. Laser scattering technology is represented by methods including Rayleigh scattering [5], spontaneous

* Author to whom any correspondence should be addressed.

Raman scattering [6], and coherent anti-Stokes Raman scattering (CARS) [7]. Although these methods offer high measurement accuracy, the experimental equipment required is quite complex and expensive, and this makes it difficult to apply these techniques outside a laboratory environment.

As a passive optical measurement method, optical emission spectroscopy does not require use of external light sources. This remarkable characteristic is highly advantageous in complex measurement environments and when performing long distance measurements. Over the past few decades, there have been numerous reports of flow field information measurements using emission spectra. In terms of atomic spectra, the intensity ratio or the slope ratio of the spectral line [8–10] and the Boltzmann diagram method [11–13] are commonly used. Unfortunately, because of the limited numbers of atomic spectral lines, non-thermodynamic equilibrium, and other factors, it is difficult to apply these methods at high temperatures and in unsteady flows. Professor Gerhard Herzberg, who won the Nobel Prize for Chemistry in 1971, performed in-depth research in the fields of electronic structures and molecular geometry that laid the foundation for the measurement technique of emission spectroscopy [14–19]. In addition, with the continuous development of spectral databases such as high resolution ransmission olecular bsorption database (HITRAN) [20] and high temperature molecular spectroscopic database (HITEMP) [21], molecular spectroscopy thermometry has also gradually become a research hotspot.

Molecular emission spectrometry thermometry mainly uses spectra produced by diatomic molecules such as $C_2{}^*$, OH^*, and CH^* from excited state to low energy level transitions to determine the temperature. In 1950, however, Gaydon found a difference with respect to the thermodynamic temperature when using the spectrum of OH^* to measure the temperature of a hydrocarbon flame [22]. Additionally, in 2011, Passaro *et al* observed the high rotation temperature phenomenon when measuring the combustion temperature of liquefied gas based on the $C_2{}^*$ emission spectrum [23]. The main reason for the observed differences in these cases is that the number distribution of the excited state particles has not reached its equilibrium state, and the rotational energy level is thus over-distributed. Fortunately, thermally excited water vapor molecules reach their equilibrium population when they are formed, and the temperature for each degree of freedom (DF) of the excited state is approximately equal to the thermodynamic temperature. In addition, Water vapor is the most common component of combustion products, And the research of water vapor spectra goes back about 100 years. In 1940, Darling and Dennison revealed the vibrational spectral structure of water vapor molecules through the semi-rigid molecular theory [24] Benedict *et al* and Gaydon obtained strong water vapor emission spectrum through the analysis of flame spectrum [25, 26]. In recent years, the radiation spectrum of water vapor has gradually shown the value of industrial application. In 2016, Ellis *et al* divided the spectrum within the same electron band system and preliminarily obtained the one-dimensional flame temperature under the assumption of uniform flame absorption rate and without considering self-absorption by combining the integral ratio of spectral intensity. At the same time, the source of measurement error is analyzed [27].

Regardless of whether atomic or molecular spectra are considered, the self-absorption phenomenon in these spectra is noteworthy. In 2003, Laux *et al* used OH^* to measure the atmospheric plasma temperature and found that self-absorption led to measurement errors. In addition, they estimated that when the self-absorption reached 4%, the temperature would then be offset by 100 K [8]. Previous work has usually defaulted to the optical thinness and ignored the self-absorption phenomenon, which is feasible for measurement of small-scale flames in the laboratory. However, in temperature measurement of larger flames, such as those encountered in aero-engine ground experiments, the presence of the self-absorption phenomenon is unavoidable.

In this paper, a method of temperature measurement based on the integral ratio of spectral intensity of water vapor emission spectrum is introduced, and the effect of self-absorption is taken into account, which provides a measurement idea for large-scale flame temperature measurement in industrial applications. We believe that this method can avoid the unavoidable problem of interference flow field in contact temperature measurement, and will obtain a wider temperature measurement range than TDLAS technology. In addition, the cost and technical difficulty of the measurement system will be much lower than CARS. These obvious advantages will make the method very suitable for the temperature detection of engine combustion chamber, and also lay a foundation for the extension of the method to multi-dimension.

2. Water vapor emission spectra at high temperature

As shown in figure 1, H_2O and CO_2 are two common components of the combustion products of hydrocarbon fuels. In addition, figure 1 shows that water vapor has a higher radiation intensity than CO_2 at the same temperature and pressure concentration above 5500 cm^{-1}, which makes it relatively easy to collect the water vapor spectrum experimentally because it will not be disturbed by the radiation from other components.

H_2O is a triatomic asymmetric top molecule and its rotational-vibrational spectrum is more complex than that of most other triatomic molecules. In 1933, Mecke *et al* provided the basic structure of water molecules and analyzed 16 vibration-rotational water vapor radiation belts in the 5650 Å–6 μm region [28]. The angle and the distance between the O–H bonds in the molecular structure of H_2O are 104° 36′ and 0.9558 Å, respectively, and like all nonlinear triatomic molecules, they have six internal degrees of freedom (three rotations and three vibrations). With regard to their vibrational modes, water molecules have three basic vibrational frequencies: $V1 = 3650\ cm^{-1}$, $V2 = 1595\ cm^{-1}$, and $V3 = 3755\ cm^{-1}$ [24].

The high-speed collisions that occur between particles in high temperature environments cause the translational, rotational, vibrational, and electronic degrees of freedom of the molecules to be excited completely. A transition between two

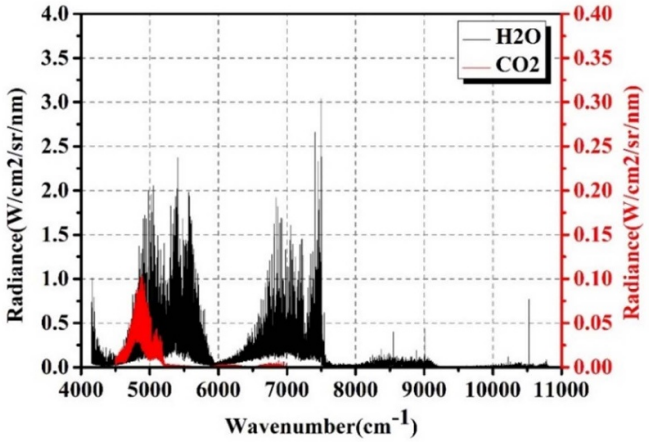

Figure 1. Comparison of calculated spectra at 2500 K, 1 atm, an optical depth of 50 mm, a H_2O concentration of 66%, and a CO_2 concentration of 33%.

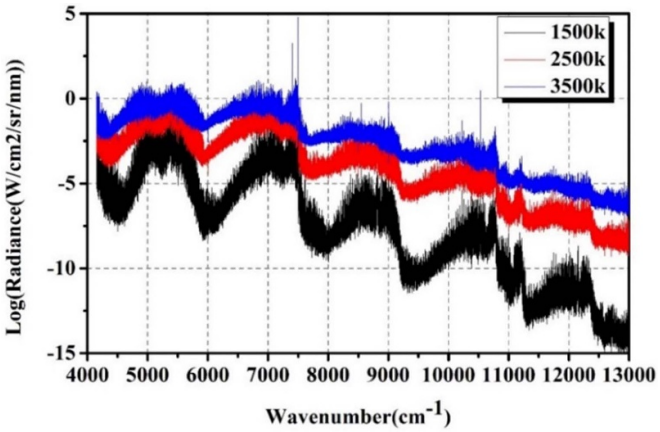

Figure 2. Comparison of calculated water vapor spectra at different temperatures (over the 4000–13 000 cm^{-1} range), where the ordinate radiation power is the logarithmic value.

electronic states results in an electron band. However, an electron band usually consists of multiple vibrational bands formed by transitions between these vibrational bands. In addition, each vibrational band includes multiple rotating branches, and this ultimately forms the basic structure of the molecular emission spectrum—the band spectrum. Regardless of whether an absorption line or an emission line is considered, the line width is not infinitely narrow, but has a specific width. These lines are subject to different broadening mechanisms, which can be divided into uniform broadening and nonuniform broadening types [29–32]. In addition to the two broadening mechanisms above, the experimental spectrum collected by the spectrometer is actually the convolution of the real spectrum and the spectrometer instrument function $\Phi(\nu)$, and it is also affected by the optical path arrangement, the responses of the optical components, and self-absorption [33, 34].

We demonstrate the correlation between spectral intensity and temperature using a simplified formula for calculating spectral intensity. Under the assumption of optical thinness, self-absorption is ignored, then the emission coefficient can be calculated using equation (1):

$$\varepsilon(\nu) = \sum \left(\frac{hc\nu^{\nu'J'}_{\nu''J''}}{4\pi} A^{\nu'J'}_{\nu''J''} N_{\nu'J'} \cdot \phi_{\nu'J'}(\nu) \right) \quad (1)$$

Here, c is the speed of light, h is Planck's constant, $\nu^{\nu'J'}_{\nu''J''}$ is the wave number of the energy level transition, $A^{\nu'J'}_{\nu''J''}$ is the probability of a spontaneous emission Einstein transition, $N_{\nu'J'}$ is the number of excited state particles, and $\phi_{\nu'J'}$ is a linear function. The number of excited particles $N_{\nu'J'}$ can be calculated using equation (2):

$$N_{\nu'J'} = \frac{N_0 g_e}{Q_e Q_v Q_r} \exp\left(-\frac{E_e}{kT_e}\right) \cdot \exp\left(-\frac{E_v}{kT_v}\right) \cdot (2J'+1) \cdot \exp\left(-\frac{E_r}{kT_r}\right) \quad (2)$$

where N_0 is the total number of molecules, k is the Boltzmann constant, E_r, E_e, and E_v are the energies of the rotational, vibrational, and electronic states, respectively. T_r, T_v, and T_e are the rotational, vibrational, and electronic temperatures, respectively. Q_r, Q_v, and Q_e are the partition functions of the rotation, vibration, and electronic states, respectively, g_e is the degeneracy of the electronic state, and J is the quantum number of the high energy level. When equations (1) and (2) are combined, it is shown that the spectral line intensity has a strong temperature dependence.

Previous experimental studies have confirmed that the intensities of the radiation spectra of gaseous combustion products, including water vapor, show a strong correlation with temperature. For example, in 1964, Breeze *et al* verified the variation in the integral intensity of the molecular vibration-rotation band with temperature in a rocket tail flame and in shock tube experiments, and also confirmed the temperature dependence of the molecular emission spectrum [35]. Figure 2 shows the emission spectra of theoretical water vapor spectral data (HITEMP2010) over the range from 4000 to 13 000 cm^{-1} at different temperatures (the optical depth was set at 50 mm, the concentration was 66%, the air pressure was 1 atm, and the spectral resolution was 0.01 cm^{-1}). It is thus obvious that temperature has a major influence on the spectral intensity and structure of the water vapor radiation. From the viewpoint of statistical thermodynamics, the concept of temperature should be associated with each DF of the particle, in addition to the temperature of advection, there are rotation temperature, vibration temperature and electron temperature, and only when the thermodynamic system is in equilibrium, the temperature of each DF is equal. Water vapor, as a molecule with a short relaxation time, can reach the equilibrium state by a smaller number of collisions in a chemical reaction, so the temperature obtained from the vibrational rotation spectrum of water vapor is the flame temperature [36].

3. Temperature measurement method based on the integral ratio of spectral intensity of two bands

As a passive optical measurement method, the emission spectroscopy measurement technique does not require external

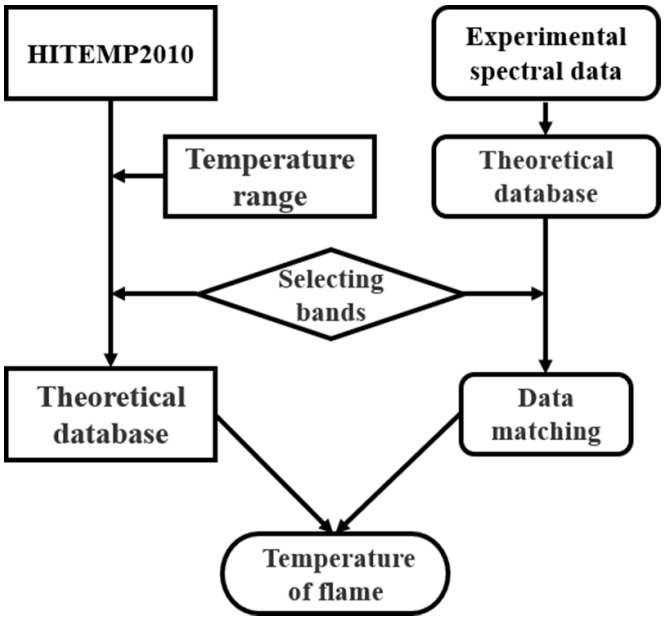

Figure 3. Flow chart for flow field temperature measurement by the band integral ratio method.

light sources to be provided and does not interfere with the flow field structure, and thus offers considerable advantages in both simplifying the experimental system required and maintaining the integrity of the flow field to be measured [37–39]. Use of emission spectroscopy for temperature measurements has been reported in many previous studies. The most commonly used method involves the use of high-resolution experimental spectroscopy and theoretical calculation of the spectral line structure to measure the flow field information. However, this method places extremely high requirements on the measurement resolution and the signal-to-noise ratio of the spectrum acquisition system, which is not conducive to practical applications in the aviation industry.

We propose a new method to determine the temperature by using the integral ratio of the spectral intensities of two bands, which can not only remove the dependence on the high-resolution spectrometer, but also can eliminate the influence of the concentration on the temperature measurements when the technique is applied to a uniform flow field. As shown in figure 3, the radiation spectra of water vapor at different temperatures are first calculated using the HITEMP database. On this basis, and by considering the temperature sensitivities of the different transition bands and the signal-to-noise ratio of the experimental spectra, the band that is most suitable for a constant temperature is selected. The curve of the integral ratio of the corresponding band of the theoretical spectrum is then solidified into a database to be queried. The integrated ratio value of the processed experimental spectral data in the corresponding band is then calculated, and the temperature of the flow field to be measured is subsequently retrieved from the database.

The two emission spectral bands used to perform the temperature measurements must follow three principles: (a) their water vapor radiation is strong when compared with their other components; (b) the spectral band is easy to measure in the experiment, and its signal-to-noise ratio is high; and (c) the slope of the band integral ratio is high enough to obtain high temperature sensitivity. To enable comparison of the differences between the different bands, four groups of theoretically calculated spectral data from experiments A to D are listed in table 1. In figure 4, the band ratio for each group is plotted as a curve that varies with temperature.

Table 1. Four arbitrarily selected groups of water vapor radiation band combinations.

Experiment number	A	B	C	D
Band 1(cm^{-1})	6660–7142	6660–7142	6660–7142	6660–7142
Band 2(cm^{-1})	10 000–10 869	8333–9259	6250–6660	5882–6250

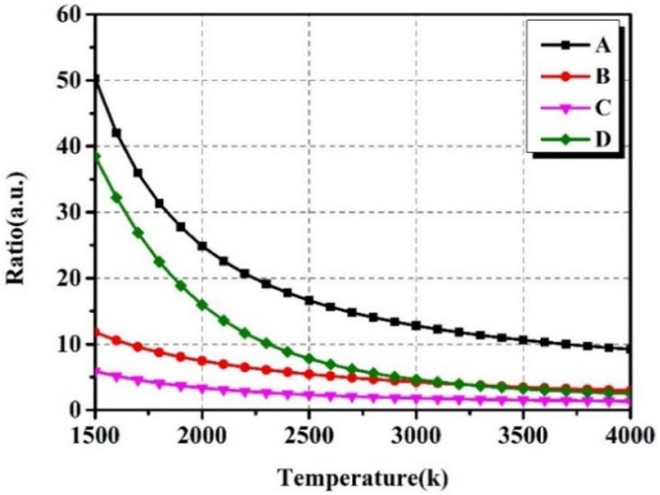

Figure 4. Variation curves of the integral ratios of four groups (A–D) with respect to temperature.

Although two different bands can be selected arbitrarily, the integral ratio in practical applications should have a larger slope with respect to temperature to ensure temperature sensitivity. At the same time, it is also necessary to take the signal-to-noise ratio of the experimental spectrum into account to ensure the accuracy of the constant temperature. Previous research has shown that the water molecules in the ranges of 6400–7600 cm^{-1} ($V1 + V3$, $V1 + V2 + V3 - V2$) and 9500–11 500 cm^{-1} ($4V2 + V3$, $2V1 + 2V2$, $V1 + 2V2 + V3$, $2V2 + 2V3$, $3V1$, $2V1 + V3$, $V1 + 2V3$) [40–42] have strong vibration bands; therefore, we selected Group A from table 1 to measure the temperature of the hot gas after methane and oxygen combustion.

4. Introduction to the experimental system

The experimental system can be divided into three modules: the burner, the flow control module, and the spectrum acquisition module. The experiment used a self-created

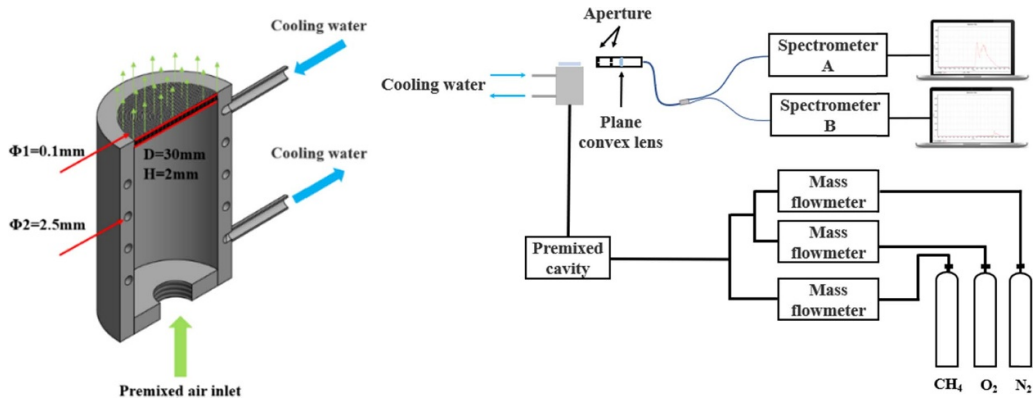

Figure 5. Burner cross-section (left side) and schematic diagram of the experimental system (right side).

laminar flow burner, which was fabricated using 3D printing technology [43, 44]. As shown in figure 5, the burner diameter is $D = 30$ mm, the burner thickness is $H = 2$ mm, and the airflow outlet is designed to contain a large number of small holes with the same diameter of $\varphi 1 = 0.1$ mm that are formed by laser drilling, where the edge distance between the small holes is 0.3 mm. In addition, water-cooling pipes with a diameter of $\varphi 2 = 2.5$ mm are distributed on the side wall of the burner, and when it is combined with a small suction pump, the burner can operate for long periods. The flow control module consists of three mass flow controllers that control the flows of methane, oxygen, and nitrogen.

The spectrum acquisition module consists of two spectrometers (with wavelength ranges of 250–1100 nm and 950–1700 nm) and a data collection terminal. It should be noted that the two spectrometers are connected via a Y-shaped optical fiber. This Y-shaped fiber is characterized by having a single incident end and two output ends, thus allowing the two spectrometers to be used together. In addition, we used two coaxial apertures and a shading sleeve in series to ensure that the solid angle remained small enough. To allow measurements to be performed at different positions, a three-axis displacement stage is used to move the fiber's incident end, and the two spectrometers are triggered synchronously using the output pulse signal from the stepper motor.

Appropriate equivalence ratio control of the plane burner is beneficial for adjustment of the flame temperature and stability. Under ideal conditions, the burner can produce a laminar flame with a thickness of 3 mm and a diameter of 30 mm, as shown in figure 6. To verify the feasibility and the accuracy of the high-temperature water vapor radiation spectral temperature measurements, the equivalence ratio was varied in this experiment by adjusting the flow ratio to obtain flames to be measured at different temperatures.

Because the linear charge-coupled device array of the optical fiber spectrometer provides different responses to different wavelength bands, and optical components such as the optical fibers and lenses will also have different transmittances at different light wavelengths, calibration experiments must be performed in the quantitative experiments. The experimental system, including the spectrometer, the optical fiber,

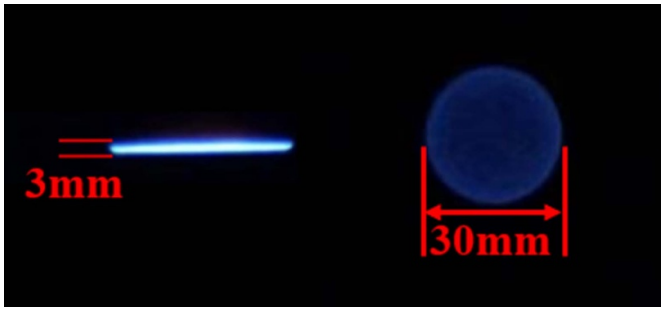

Figure 6. 3D printed-laser drilled plane furnace methane-oxygen laminar flame.

the focusing lens, and the light shielding sleeve, is calibrated and cured using a standard tungsten light source (ORIEL), Calibrated by National Institute of Standards and Technology, this tungsten lamp can be calculated by adjusting the voltage and current results to obtain the radiated power at a specific spatial location [45]. As shown in figure 7, by comparing the theoretical radiation curve for the tungsten lamp with the spectrometer's response curve, correction parameters are obtained for the entire spectrum acquisition system, i.e. the conversion relationship between the spectrometer parameters and the absolute radiation power is determined.

The experimental conditions are presented in table 2. We set three equivalence ratios to verify the reliability and sensitivity of the temperature measurements.

5. Measurement results for one-dimensional temperature of methane flame

As shown in figure 8, the spectral data for cases 1–3 were obtained by moving the lens along the furnace surface using the displacement stage. In order to improve the signal-to-noise ratio of the data, we used the integration time of up to 2000 ms(visible band) and 50 ms (near infrared band). In addition, affected by the resolution of the spectrometer and the noise of the instrument, the original spectrum was

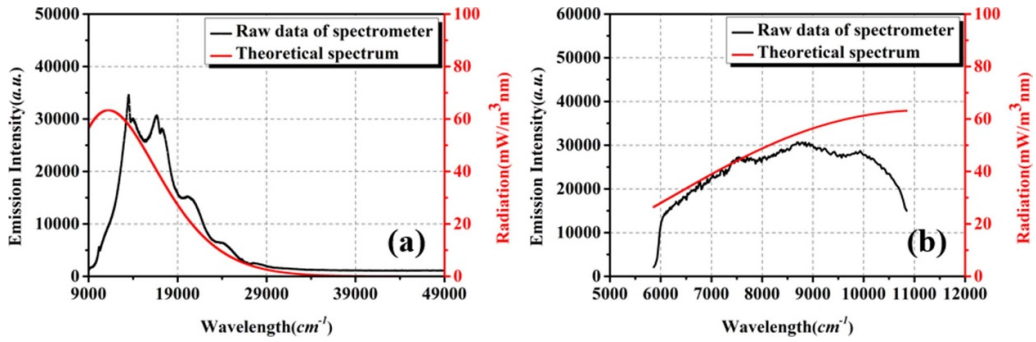

Figure 7. (a), (b) Calibration data for two spectrometers with different wavelength bands, where the red line is the theoretical radiation curve for the tungsten lamp, and the black line is the spectrometer's response curve.

Table 2. Methane, oxygen, and nitrogen flows in cases 1–3.

Experiment number	Case 1	Case 2	Case 3
O_2 (l min^{-1})	1.0	0.8	0.7
CH_4 (l min^{-1})	0.5	0.5	0.5
N_2 (l min^{-1})	0	0.2	0.3

superimposed with a spectral baseline of certain intensity, and the spectral baseline was removed by polynomial fitting.

According to the spectral data obtained, with the exception of the chemiluminescence caused by the transitions of excited state groups such as OH^* and CH^*, the main structure of the spectrum is the water vapor spectrum. In addition, because the burner was manufactured using 3D metal printing technology, atomic radiation from Na^+ (16 978 cm^{-1}) and K^+ (13 046 cm^{-1}) also exists, but the effect of this radiation on the spectral structure is small. In the third section, we proposed that the selection of the spectral bands should follow three principles. Based on the experimental spectrum obtained, we can verify that group A represents the most reasonable choice.

It is difficult to achieve a uniform flow field in engine applications. Usually, the self-absorption rate in the flow field is dependent on multiple parameters, including the temperature and concentration. Even in high-temperature flames, large numbers of ground-state particles are still present, and thus when compared with the area close to the detector, photons released by the radiation transition in the more distant flame will be absorbed by the ground-state particles along the way. As the flame increases in size, the optical path length of the distant photons also increases, and the absorption that occurs along this path also strengthens. Because the plane laminar flow flame burner is used in the experiment and it is small in size, it can be simplified as a uniform flow field when self-absorption is considered, i.e. the absorption rate for the self-absorption is the same everywhere in the flow field. We propose use of ray tracing to add the self-absorption effect of the flame to the temperature measurement process [46, 47].

It is obvious that the spectra collected in the experiment are the real spectra coupled with the self-absorption, so the influence of self-absorption must also be taken into account when obtaining the temperature-intensity curve of the theoretical spectrum. As shown in figure 9, it is assumed that the total length of the flame area is L, the selected micro-element is dL, the incident light intensity on the left side of the micro-element is $I_0(L, V)$, and the outgoing light intensity on the right side is $I(L, V)$. The variation dI generated by the incident light passing through the flame element can then be calculated using equation (3). By integrating equation (3) over the flame area, the total radiant light intensity of the uniform flow field when the self-absorption effect is considered can be obtained as shown in equation (4) [48]

$$dI(L,\upsilon) = \varepsilon(\upsilon)dL - I_0(L,\upsilon)\cdot K(\upsilon)\cdot dL \tag{3}$$

$$I(L,\upsilon) = \frac{\varepsilon(\upsilon)}{K(\upsilon)}(1-\exp(-K(\upsilon)\cdot L)) \tag{4}$$

where L is the length of the flame region, v is the wavelength, and ε and K are the emission coefficient and the absorption coefficient, respectively. It is important to note that in the calculation of theoretical spectra, all micro-elements are considered to be optically thin and self-absorption is only considered in the transmission between micro-elements. At this time we get the corrected experimental spectrum and the theoretical spectrum temperature—intensity curve considering self-absorption.

Theoretically, the adiabatic flame temperature for equivalent combustion of methane and oxygen with a laminar premix flame should be 3050 K. However, the flame temperature is affected by heat convection loss to the surrounding air and the heat conduction loss of the burner, which means that the flame temperature is lower than the adiabatic flame temperature. Figure 10 shows the measured temperature values for cases 1, 2, and 3 when self-absorption is considered and the differences between these cases and the corresponding cases without consideration of self-absorption. Even when the furnace diameter is only 30 mm, a temperature difference of nearly 3 K is observed under all three working conditions. Therefore, if this method is applied to a large-size flame, it is essential to consider the influence of the self-absorption effect on the temperature measurements.

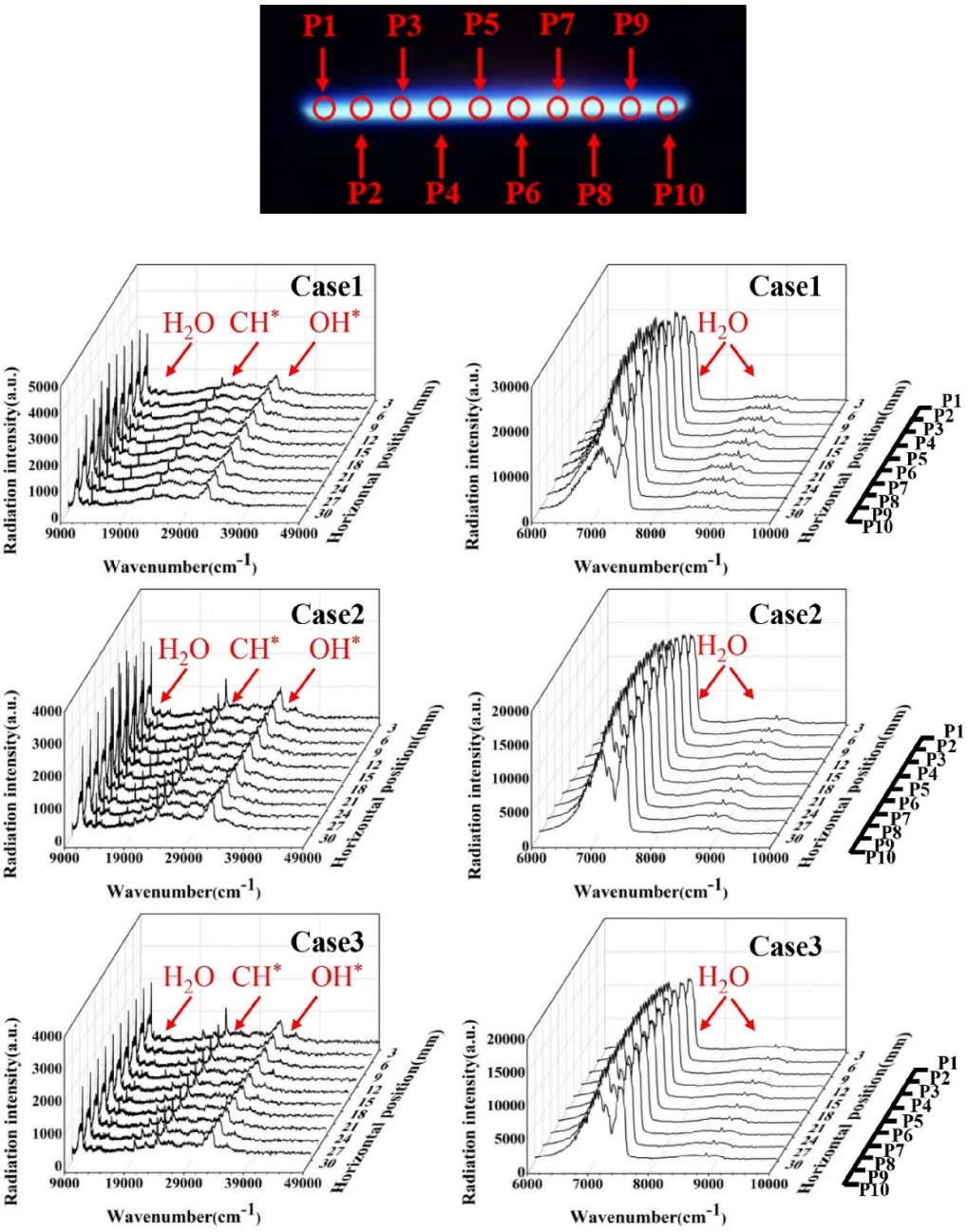

Figure 8. Acquisition position of the spectrum, and water vapor emission spectra of P1–P10 in Case 1–3.

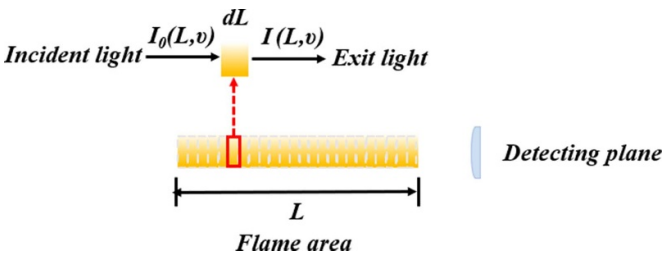

Figure 9. Schematic diagram of fiber propagation when the self-absorption effect is considered.

The average temperatures for the three operating conditions illustrate that the method can detect changes in the flame temperature even when there is a small equivalence ratio change. The equivalence ratio corresponding to case 1 is 1.0, which means that the temperature in the middle position in the furnace, i.e. the area in the horizontal position range of 12–24 mm, is higher, and the temperature on either side is lower. Case 2 and case 3 (rich fuel) show the opposite characteristics, where the temperature in the middle area is low and the temperatures on both sides are high, which occurs because of local temperature increases caused by the reaction between the fuel at the edge and the oxygen in the air in the rich combustion case.

In this experiment, because of the small size of the flame, the temperature measurement error caused by self-absorption is much smaller than the error caused by the experimental system. In this experiment, a tungsten lamp was used as a standard light source with an uncertainty of 1.1%–2.1%

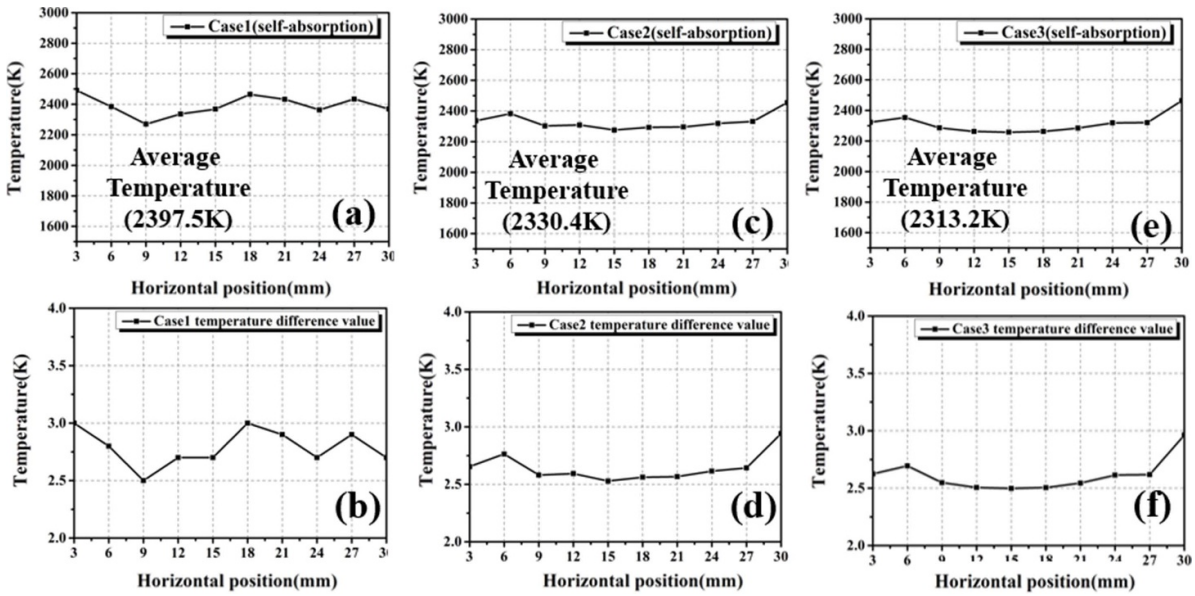

Figure 10. (a), (c), (e) Temperature measurement results and average temperatures at different positions for the three working conditions. (b), (d), (f) The temperature difference when self-absorption is considered is higher than that without self-absorption in each case.

(by two standard deviation estimates) at a calibration distance of 500 mm. Overall, the temperature measurement error is within 50 K. It should be noted here that the proposed temperature measurement method does not require complex experimental equipment. Therefore, it is an ideal temperature measurement method for use in engine combustion chamber temperature detection and other high-temperature industrial applications.

6. Conclusion

As the main component of many combustion products, the thermal excitation spectra of water vapor can be collected easily in experiments. The spectral band integral ratio temperature measurement method based on high-temperature water vapor is a passive optical measurement method that does not interfere with the flow field to be measured. In addition, the greatly simplified experimental system makes it easy to perform experimental measurements in various industrial environments.

On the basis of solving for the self-absorption effect of the flame and the equipment error, the temperature of a methane flame was measured successfully, thus laying a foundation for performance of multi-dimensional temperature measurement experiments.

Data availability statement

All data that support the findings of this study are included within the article (and any supplementary files).

Acknowledgments

We thank Professor D C M van den Bekerom from the Department of Mechanical and Aerospace Engineering, The Ohio State University, USA, for his guidance and advice on the spectral calculations. We thank David MacDonald, MSc, from Liwen Bianji (Edanz) (www.liwenbianji.cn/) for editing the English text of a draft of this manuscript.

Conflict of interest

The authors declare no conflicts of interest.

Funding

This work was supported by: the Key-Area Research and Development Program of Guangdong Province [Grant No. 2021B0909060004]; and the National Natural Science Foundation of China [Grant Nos. 12072355, 11802315, 11927803].

ORCID iD

Gongxi Zhou https://orcid.org/0000-0003-1113-8817

References

[1] Shui C, Huang J, Liu H, Cai W and Sanders S T 2021 Tomographic absorption spectroscopy based on dictionary learning *Opt. Express* **29** 36400–16
[2] Qi Q, Hossain M M, Li J J, Zhang B, Li J and Xu C-L 2021 Approach to reduce light field sampling redundancy for flame temperature reconstruction *Opt. Express* **29** 13094–114
[3] Rieker G B, Jeffries J B and Hanson R K 2009 Calibration-free wavelength-modulation spectroscopy for measurements of gas temperature and concentration in harsh environments *Appl. Opt.* **48** 5546–60

[4] Liu X, Jeffries J B, Hanson R K, Hinckley K M and Woodmansee M A 2006 Development of a tunable diode laser sensor for measurements of gas turbine exhaust temperature *Appl. Phys.* B **82** 469–78

[5] Miles R B, Lempert W R and Forkey J N 2001 Laser rayleigh scattering *Meas. Sci. Technol.* **12** R33

[6] Long D A 1977 *Raman Spectroscopy* (New York: McGraw-Hill)

[7] Eckbreth A C 1980 CARS thermometry in practical combustors *Combust. Flame* **39** 133–47

[8] Laux C O, Spence T G, Kruger C H and Zare R N 2003 Optical diagnostics of atmospheric pressure air plasmas *Plasma Sources Sci. Technol.* **12** 125–38

[9] Van Gessel A F H, Hrycak B, Jasinski M, Mizeraczyk J, Van Der Mullen JJ and Bruggeman PJ 2012 Temperature fitting of partially resolved rotational spectra *J. Instrum.* **7** C02054

[10] Bruggeman P J, Verreycken T, González M Á, Walsh J L, Kong M G, Leys C and Schram D C 2010 Optical emission spectroscopy as a diagnostic for plasmas in liquids: opportunities and pitfalls *J. Phys. D: Appl. Phys.* **43** 124005

[11] Yang Q S, Song J H and Zhu N Y 2012 Determination of temperatures using CH radical emission spectroscopy *Chin. Phys. Lett.* **29** 104707

[12] Bruggeman P J, Schram D C, Kong M G and Leys C 2009 Is the rotational temperature of OH (A–X) for discharges in and in contact with liquids a good diagnostic for determining the gas temperature? *Plasma Process. Polym.* **6** 751–62

[13] Du Y J, Tamura K, Moore S, Peng Z, Nozaki T and Bruggeman P J 2017 CO ($B1\Sigma+\rightarrow A1\Pi$) angstrom system for gas temperature measurements in CO_2 containing plasmas *Plasma Chem. Plasma Process.* **37** 29–41

[14] Herzberg G and Spinks J W T 1944 *Atomic Spectra and Atomic Structure* (Courier Corporation)

[15] Herzberg G 1951 Molecular spectra and molecular structure I. Spectra of diatomic molecules *Am. J. Phys.* **19** 390–1

[16] Herzberg G 1945 *Molecular Spectra and Molecular Structure II. Infrared and Raman Spectra of Polyatomic Molecules* (New York: D. Van Nostrant Co. Inc.) p 178

[17] Herzbergb G 1967 *Molecular Spectra and Molecular Structure III. Electronic Structure and Electronic Spectra of Polyatomic Molecules* (New York: van Nostrand Reinhold)

[18] Huberkp H 1979 *Molecular Spectra and Molecular Structure (IV): Constants of Diatomic Molecules* (New York: van Nostrand)

[19] Herzberg G 1971 *The Spectra and Structures of Simple Free Radicals: An Introduction to Molecular Spectroscopy* (Courier Corporation)

[20] Francois F 2009 The HITRAN 2008 molecular spectroscopic database

[21] Rothman L S, Gordon I E, Barber R J, Dothe H, Gamache R R, Goldman A, Perevalov V I, Tashkun S A and Tennyson J 2010 HITEMP, the high-temperature molecular spectroscopic database *J. Quant. Spectrosc. Radiat. Transfer* **111** 2139–50

[22] Gaydon A G and Wolfhard H G 1949 Spectroscopic studies of low-pressure flames. II. Effective translational and rotational temperatures from CH bands *Proc. R. Soc.* A **199** 89–104

[23] Passaro A, Carinhana J D, Gonçalves E A, Silva M M D, Guimarães A P L, Abe N M and Santos A M D 2011 The use of molecular spectra simulation for diagnostics of reactive flows *J. Aerosp. Technol. Manage.* **3** 13–20

[24] Darling B T and Dennison D M 1940 The water vapor molecule *Phys. Rev.* **57** 128–39

[25] Benedict W S, Bass A M and Plyler E K 1954 Flame-emission spectrum of water vapor *J. Res. Natl Bur. Stand.* **52** 161

[26] Gaydon A G 1942 2. The emission spectrum of water as observed in flames *Q. J. R. Meteorol. Soc.* **68** 200–1

[27] Ellis D J, Solovjov V P and Tree D R 2016 Temperature Measurement Using Infrared Spectral Band Emissions From H_2O *J. Energy Resour. Technol.* **138** 042001

[28] Mecke R, Baumann W and Freudenberg K 1933 *Z. Naturforsch.* **81** 445–65

[29] Mukamel S 1982 Collisional broadening of spectral line shapes in two-photon and multiphoton processes *Phys. Rep.* **93** 1–60

[30] Faid K 1986 Stochastic theory of relaxation and collisional broadening of spectral line shapes (Georgia Institute of Technology)

[31] Wilamowski Ż, Przybylińska H and Jantsch W 1995 Mechanisms of nonuniform line broadening *Acta Phys. Pol.* A **87** 181–4

[32] Hodges J T, Lisak D, Lavrentieva N, Bykov A, Sinitsa L, Tennyson J, Barber R J and Tolchenov R N 2008 Comparison between theoretical calculations and high-resolution measurements of pressure broadening for near-infrared water spectra *J. Mol. Spectrosc.* **249** 86–94

[33] Dulov E N and Khripunov D M 2008 Instrumental broadening of spectral line profiles due to discrete representation of a continuous physical quantity *J. Quant. Spectrosc. Radiat. Transfer* **109** 1922–30

[34] Bertrand P 2020 How instrumental parameters affect the shape and intensity of the spectrum *Introduction to Simulation Methods*

[35] Breeze J C, Ferriso C C, Ludwig C B and Malkmus W 1965 Temperature dependence of the total integrated intensity of vibrational—Rotational band systems *J. Chem. Phys.* **42** 402–6

[36] Fiévet R, Voelkel S, Koo H, Raman V and Varghese P L 2017 Effect of thermal nonequilibrium on ignition in scramjet combustors *Proc. Combust. Inst.* **36** 2901–10

[37] Chun L, Lu-Dong Z, Yang P Zhongnong Z H, Zhicong L I and Pengfei C H 2021 Research progress of passive combustion diagnosis technology based on spontaneous radiation analysis *J. Exp. Fluid Mech.* **35** 17

[38] Ballester J and Garcia-Armingol T 2010 Diagnostic techniques for the monitoring and control of practical flames *Prog. Energy Combust. Sci.* **36** 375–411

[39] Gaydon A G 1974 *The Spectroscopy of Flames* (Chapman & Hall)

[40] van den Bekerom D C M and Pannier E 2020 A discrete integral transform for rapid spectral synthesis *J. Quant. Spectrosc. Radiat. Transfer* **261** 107476

[41] Camy-Peyret C, Flaud J M, Maillard J P M and Guelachvili G 1977 Higher ro-vibrational levels of H_2O deduced from high resolution oxygen-hydrogen flame spectra between 6200 and 9100 cm^{-1} *Mol. Phys.* **33** 1641–50

[42] Tolchenov R N, Tennyson J, Brault J W, Canas A A D and Schermaul R 2002 Weak line water vapor spectrum in the 11787–13554 cm −1 region *J. Mol. Spectrosc.* **215** 269–74

[43] Buchanan C and Gardner L 2019 Metal 3D printing in construction: a review of methods, research, applications, opportunities and challenges *Eng. Struct.* **180** 332–48

[44] Rajasegar R, Mitsingas C M, Mayhew E K, Liu Q, Lee T and Yoo J 2017 Development and Experimental characterization of metal 3D-printed scalable swirl stabilized mesoscale burner array *ASME 2017 Int. Mechanical Engineering Congress and Exposition*

[45] Teng F, Congyuan P, Qiang Z, Xuewei D and Qiuping W 2018 Calibration of absolute efficiency of laser induced

breakdown spectroscopy using halogen tungsten lamp *Acta Photonica Sin.* **47** 23–30

[46] Du Y J, Nayak G, Oinuma G, Ding Y, Peng Z and Bruggeman P J 2017 Emission considering self-absorption of OH to simultaneously obtain the OH density and gas temperature: validation, non-equilibrium effects and limitations *Plasma Source Sci. Technol.* **26** 095007

[47] Du Y J Peng Z M and Ding Y2017 Calibration-free optical emission spectroscopy method for the measurements of gas temperature and OH density *OSA Conf. Applied Industrial Optics*

[48] Hanson R K, Spearrin R M and Goldenstein C S 2016 *Spectroscopy and Optical Diagnostics for Gases* (Springer International Publishing)